



The Open Mechanical Engineering Journal

Content list available at: <https://openmechanicalengineeringjournal.com>



RESEARCH ARTICLE

Wear and Corrosion Resistance of Hardened Fe-Al-Mn Grinding Ball

Ratna Kartikasari^{1,*}, Adi Subardi¹ and Anita Susiana¹

¹Department of Mechanical Engineering, Institut Teknologi Nasional Yogyakarta, Jl. Babarsari No.1 Caturtunggal, Depok, Sleman, Yogyakarta, Indonesia

Abstract:

Objective:

This study aimed to determine the effect of hardening temperature on microstructure, wear and corrosion resistance of Fe-Al-Mn alloy grinding ball.

Methods:

Hardening process was carried out at 900°C, 950°C, 1000°C, 1050°C and 1100°C, held for 60 minutes and cooled using SAE 20 oil. Tests included chemical composition, SEM-EDS, wear and corrosion resistance test.

Results:

Chemical composition test results show that this alloy is high alloy steel because it contains 3.6% aluminum (Al), 13.6% manganese (Mn) and 1.1% carbon (C). Microstructures found are austenite, ferrite and kappa. EDS test results show that in the austenite phase, C decreased when hardening temperature increased. Ferrite phase contains Mn which increased when hardening temperature increased while C was the other way around. Mn is relatively stable in the kappa phase. The best wear and corrosion resistance (4.3×10^{-7} mm²/kg and 0.00026 mm/yr) of hardened Fe-Al-Mn grinding ball occurred at 900°C. The corrosion rate is extraordinary.

Conclusion:

Microstructures of the Fe-Al-Mn alloy grinding ball after the hardening process are austenite, ferrite and kappa.

Keywords: Grinding ball, Fe-Al-Mn alloy, Hardening, Corrosion resistance, Corrosion rate, High alloy steel.

Article History

Received: February 04, 2020

Revised: April 27, 2020

Accepted: May 12, 2020

1. INTRODUCTION

Grinding in a milling machine is an essential technological process to reduce the size of particles which may have different nature and a wide diversity of physical, mechanical and chemical characteristics. Milling machines have been extensively applied in various fields such as mining, chemical and pharmaceutical industries [1 - 3]. One of the most popular milling machines is cement mill, which is used to crush raw materials using grinding balls. The raw materials are limestone (supplies the bulk of the lime), clay, marl or shale (supplies the bulk of the silica, alumina and ferric oxide) and other supplementary materials, such as sand, fly ash/Pulverized Fuel Ash (PFA), or iron stone to achieve the desired bulk composi-

tion [4]. Therefore, grinding balls must have characteristics such as wear and corrosion resistance.

The use of balls in grinding ores is a major factor in determining the cost of milling operations. It has been known that mechanisms of abrasion, corrosion and impact contribute to total wear of grinding balls. However, it is hard to isolate the contribution of each mechanism towards total media wear [5]. It is estimated that more than half of the grinding media wear is caused by corrosion or dissolution of the active nascent metal surfaces continuously exposed during grinding [6].

In general, grinding balls used in cement industries are made of high chromium cast iron in the form of martensitic, pearlitic and austenitic matrices [7, 8]. Chromium as the main element is strategic and expensive due to its limited reserve in the world. Therefore, it is necessary to find an alternative to replace it. One candidate to replace Cr is Al because of its similar effects on iron, like stabilizing ferrite, increasing

* Address correspondence to this author at the Department of Mechanical Engineering, Institut Teknologi Nasional Yogyakarta, Jl. Babarsari No.1 Caturtunggal, Depok, Sleman, Yogyakarta, Indonesia; Tel: +62274 485390; E-mail: ratna@itny.ac.id

mechanical properties and corrosion resistance [9, 10].

Many researchers have extensively investigated Fe–Al–Mn–C alloys because of their superior features, such as low density, low magnetism, high strength, high ductility, and good biocompatibility [11 - 18]. The increase of Stacking Fault Energy (SFE) because of the addition of Al significantly influences the deformation twinning and strain hardening behaviors of Fe–Mn–Al–C steels with <6 wt% Al [19 - 21]. However, even though the addition of Al content (~ 9wt%) improves the strength, it significantly decreases the strain hardening rate of the steel [22]. It is proven that the addition of Al significantly enhances the formation of nanoscale (Fe,Mn)₃AlC κ -carbide precipitates, which also remarkably influences the mechanical properties and deformation behavior of aged Fe–Mn–Al–C steels [23].

To improve the intrinsic mechanical properties of the FeAl alloys, manganese and carbon additions seem promising because manganese and carbon stabilize the austenitic domain allowing it to achieve an alpha/gamma phase transformation in the otherwise totally ferritic Fe–Al alloy [24]. The addition of Mn in the Fe–Al alloy system will stabilize the austenite structure and increase hot workability and ductility [10]. α/γ duplex microstructure can be obtained if manganese content is less than 10 at% while structural hardening and total stabilization of the austenite occurred if manganese content is above 10 at% [25].

Even though there has been much research focused on Fe–Al–Mn alloy for substituting Fe–Cr–Ni as stainless steel, the study on Fe–Al–Mn alloy for the grinding ball has not been found. If this research proves that the Fe–Al–Mn alloy can replace the grinding ball of the Fe–Cr alloy, it will be very economically beneficial because the world reserves of Al are very abundant and the price is relatively cheap, besides that the Fe–Al–Mn alloy is superior in mechanical properties and corrosion resistance. This research aimed to develop this alloy for grinding ball by applying a hardening process to improve its hardness (wear resistance) and corrosion resistance.

2. MATERIALS AND METHODS

The chemical composition of the Fe–Al–Mn grinding balls studied in this work is shown in Table 1. The alloy was prepared using an induction furnace under argon atmosphere. Fe–Mn medium C, mild steel scrap, high purity aluminum, and Fe–C were used as raw materials. Thirty-five kilograms of molten metal was poured into grinding balls molds with diameter 15 mm, 20 mm and 30 mm. The grinding balls were cut to the size fit for each test using a water cooling cutting machine. The hardening process was carried out at 900°C, 950°C, 1000°C, 1050°C and 1100°C using muffle furnace within 1 hour, followed by cooling in oil SAE 10. The element content of each phase in the grinding ball was examined using JEOLJSM 6510 LA EDS equipment using CuK α radiation. Phases and wear resistance were examined using Rigaku Multiflex 2 kw XRD equipment and Ogoshi Methode respectively. Corrosion resistance was examined using PGS-201T potentiostat corrosion testing within 2.5% HCl

solution media.

3. RESULTS AND DISCUSSION

3.1. Microstructure Analysis

Fig. (1) shows that Fe–Al–Mn alloy grinding ball raw material has a duplex austenite–ferrite microstructure [23]. The Austenite phase serves as a matrix while the ferrite phase is distributed evenly with a random pattern. The small amount of ferrite phase observed is caused by Al content 3.63 wt% which serves as ferrite stabilizer. As an austenite stabilizer 13.6 wt% Mn element dominantly generates the formation of austenite phase, as shown in the Schaeffler diagram [26]. Kappa phase is not observed between these two phases.

Table 1. Compositions of Fe–Al–Mn Alloy grinding ball.

Elements	Al	Mn	C	Si	Cr	Ni	Mo	V	P
Contents (wt%)	3.63	13.6	1.12	0.81	0.29	0.02	0.01	0.09	0.07

The hardening process at 900°C increases the ferrite phase. Thermal agitation stimulated motions of atoms in Fe–Al–Mn alloy causing FCC disordered becomes FCC ordered [27]. This process continued, and later a few atoms of Fe, Al, Mn arranged themselves forming the kappa phase. Fig. (2a) shows the kappa phase surrounding the ferrite phase (ring-like) which is light grey [23]. At 950°C thermal agitation increased causing more atoms to transform into the kappa phase. It is shown in Fig. (2b) that the light grey layers around the ferrite phase are thicker. In the meantime, ferrite expanded and merged forming a clumped pattern which is dark grey as shown in Fig. (2b). The increase in hardening temperature tends to increase thermal agitation activity. Figs. (2c–e) show a bigger ferrite phase and thicker kappa layers.

The microstructure of “high Mn” alloy consists of three phases: the ferrite matrix, kappa precipitates and the austenitic phase. In this kind of alloy, the kappa precipitate surrounds as a thin border (from 1 to 5 μ m thick) the thick homogeneous austenitic phase (from 10 to 20 μ m thick) [23].

3.2. EDS Analysis

Fig. (3) shows the EDS result of Fe–Al–Mn grinding ball. Equilibrium content of elements is calculated as the average of element content in each phase. The hardening process causes a decrease of Mn content in the austenite phase. On the contrary, the process causes the increase of Mn content in the ferrite phase. The higher the hardening temperature, the lower Mn content in the austenite phase and the higher Mn content in the ferrite phase are. Al content, on the other hand, increases in the austenite phase and decreases in the ferrite phase. Carbide precipitation increases as hardening temperature increases.

These microprobe analyses give us one tie-line of the quaternary equilibrium phase diagram at 900°C. Table 2 shows the manganese contents are highest in the austenite phase while the aluminum content is highest in the kappa phase. After the hardening process, manganese and aluminum content in the austenite phase increases followed by a decrease in the ferrite and kappa phase.

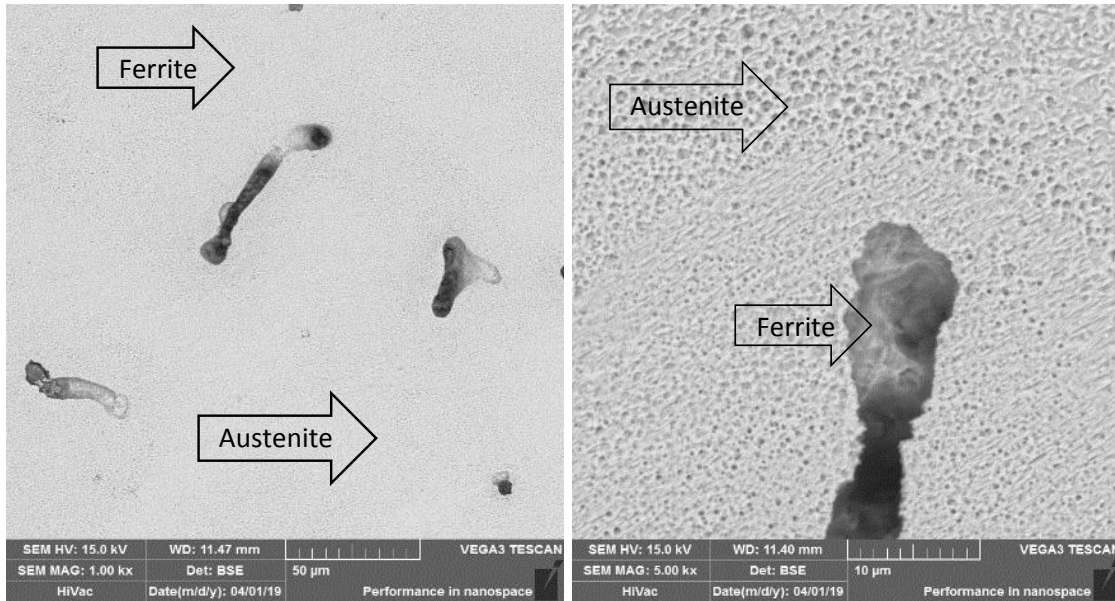


Fig. (1). Microstructures of raw material Fe-Al-Mn grinding ball.

Table 2. The phase composition of Fe-Al-Mn grinding ball

Fe-Al-Mn Grinding Ball	Austenite		Ferrite		Kappa	
	Mn (wt%)	Al (wt%)	Mn (wt%)	Al (wt%)	Mn (wt%)	Al(wt%)
Raw Material	16.1	1.2	10.5	4.2	14.2	5.49
Hardened	18.1	1.34	9.75	4.07	12.95	5.39

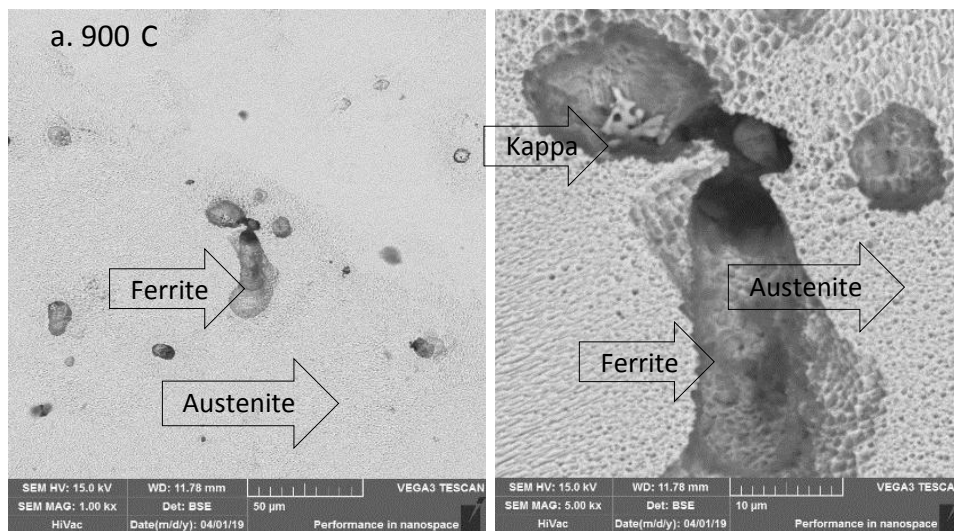


Fig. 2 cont.....

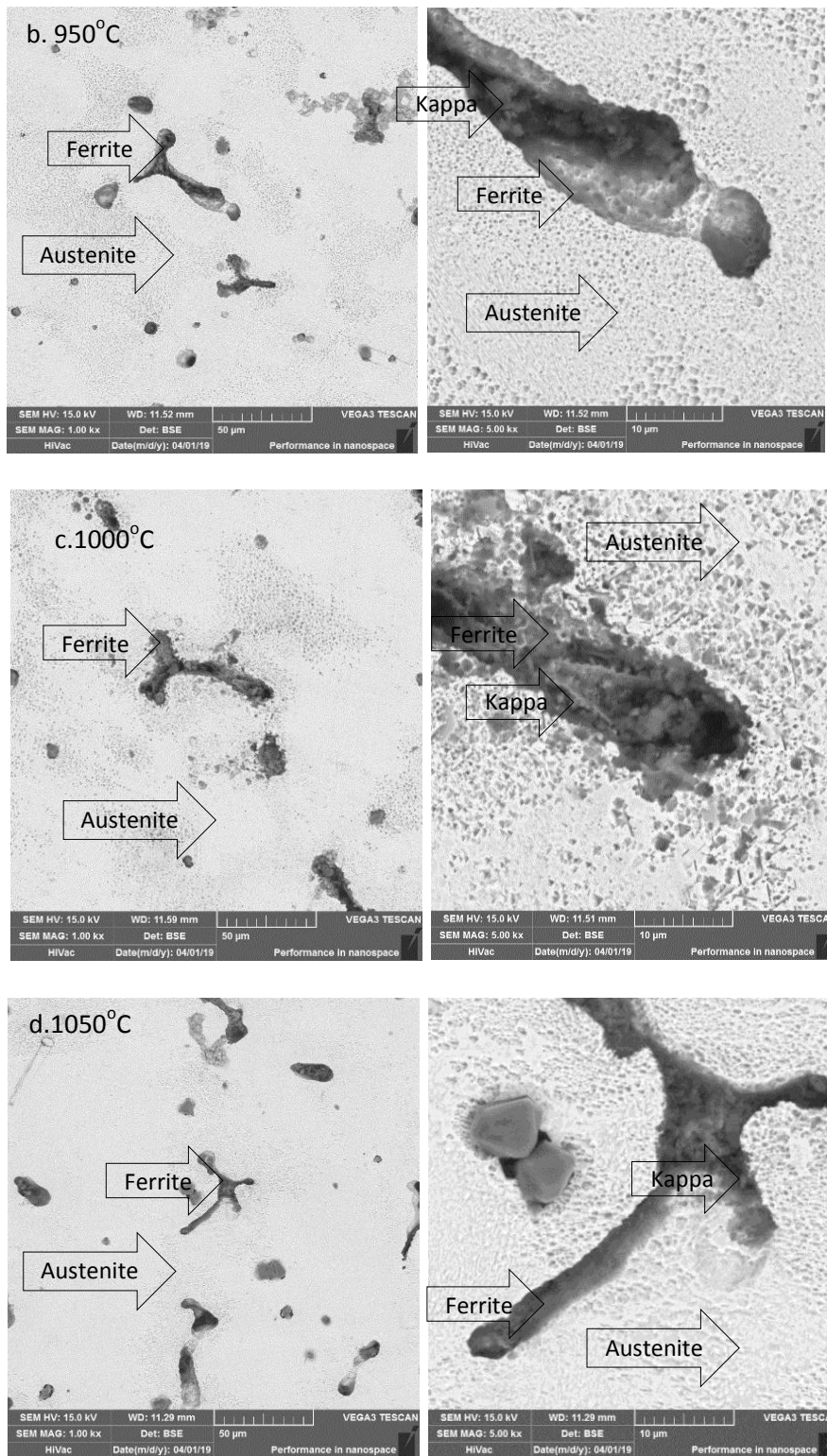


Fig. 2 cont.....

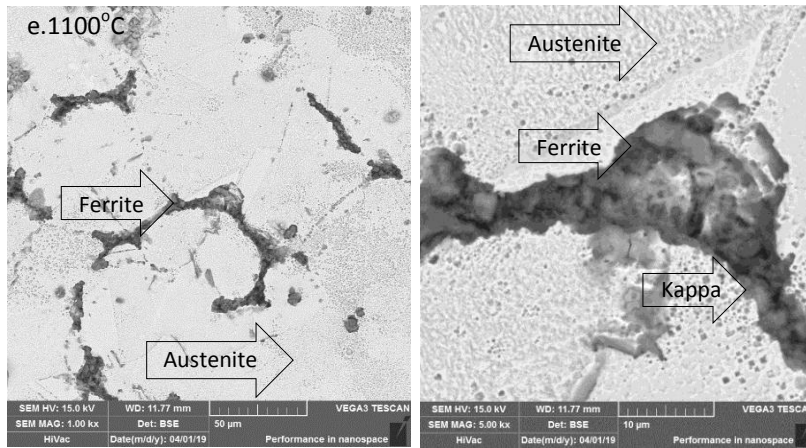


Fig. (2). Microstructures of hardened Fe-Al-Mn grinding ball.

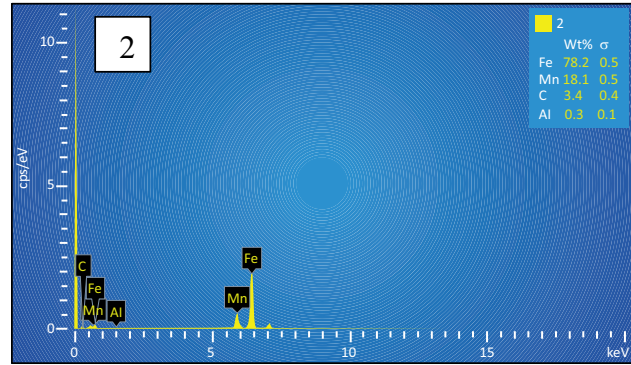
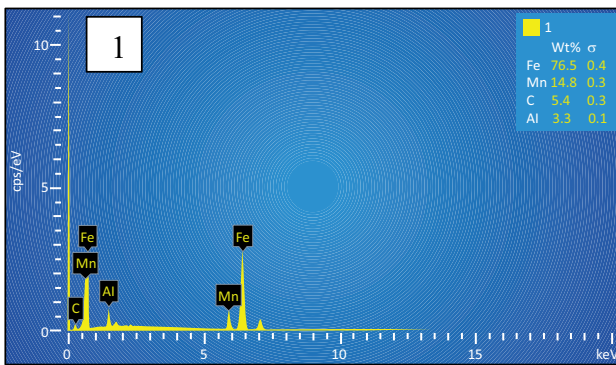
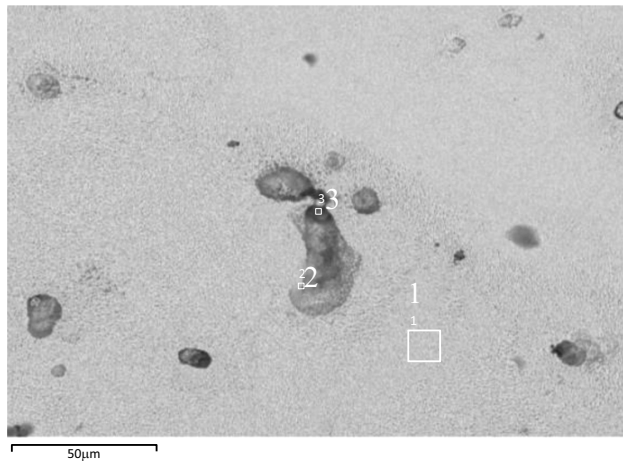


Fig. 5 cont.....

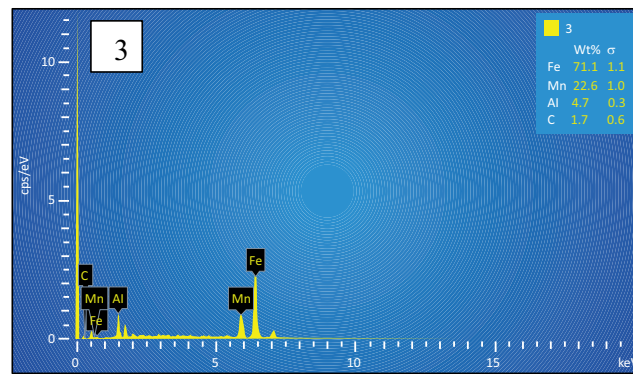


Fig. (3). EDS result of 900°C hardened Fe-Al-Mn grinding ball.

At 900°C, for the “low Mn” alloy, manganese and aluminum contents are higher in the kappa phase than in the ferrite matrix. For the “high Mn” alloy, manganese content is higher in the austenitic phase than in the ferrite matrix while aluminum content is lower [23].

3.3. Wear Resistance Analysis

Wear resistance was examined using Ogoshi Universal High Speed Wear Testing. Specific wear is measured by calculating the width of wear on an object test conducted by a dish spinning. Specific wear is calculated by the equation:

$$Ws = \frac{B \cdot bo^3}{8 \cdot r \cdot Po \cdot lo} \left(\frac{mm^2}{kg} \right)$$

Where,

Ws = specific wear (mm^2 / kg)

B = width of the saucer (mm)

bo = width of specimen wear (mm)

r = radius of the disk (mm)

Po = force on the wear process (kg)

Lo = mileage on the wear process (m)

Fig. (4) shows the relation between hardening temperature and wear of Fe-Al-Mn grinding ball. It can be seen that the higher the hardening temperature, the lower its wear rate. It means the wear resistance of Fe-Al-Mn grinding ball increases. It is resulted by the changes of its microstructure during the hardening process in which recrystallization followed by the growth of austenite grain occurred. Recrystallization is more perfect and the austenite grains are bigger when hardening temperature is higher. When sudden cooling is applied, the growth of austenite grains is stopped, the atoms are arranged in an FCC disordered pattern. At higher temperature, FCC disordered lattice is shorter so that the crystal density is higher because the cooling rate is faster and vice versa. Simultaneously, austenite grains are finer, kappa phase is formed and ferrite structure decreases. The highest wear rate $1.1 \times 10^{-6} mm^2/kg$ occurs at raw material specimen while the lowest wear rate $4.3 \times 10^{-7} mm^2/kg$ occurs at the specimen after

hardening at 900°C.

3.4. Corrosion Resistance Analysis

The quantitative value of the corroded metal is calculated using the corrosion equation expressed in mm/yr.

$$CR = 0,129 \frac{I_{corr} (EW)}{\rho}$$

Where,

CR = Corrosion Rate (mpy)

Icorr = current density ($\mu A/cm^2$)

EW = Equivalent Weight (g/equivalent)

ρ = density (g/cm^3)

Equivalent weight is calculated using the following equation [28]:

$$EW = N_{EQ} e^{-1}$$

$$N_{EQ} = \sum \left[\frac{n_i f_i}{a_i} \right]$$

Where,

EW = Equivalent Weight

N_{EQ} = total number of equivalent

n_i = atomic weight

f_i = weight fraction

a_i = valence

Fig. (5) shows that the corrosion rate of Fe-Al-Mn alloy grinding ball raw material is 0.0031 mm/yr which is categorized as very good [29]. The hardening process at 900°C resulted in a significant decrease in the corrosion rate up to 91.6% (0.00026 mm/yr). It was triggered by the formation of Al_2O_3 oxide layers on the surface of the alloy and microstructure changes as a result of the heating process followed by rapid cooling. Kappa phase was formed around the ferrite phase, however, at the same time, the existing ferrite phase grew in a very small percentage. The higher the hardening temperatures, the higher the corrosion rate of Fe-Al-

Mn alloy grinding ball. At 950°C, the corrosion rate increased significantly as much as 73%. At 1000°C corrosion rate reached 0.00066 mm/yr or in other words, it increased by 32%. The highest corrosion rate (0.00097 mm/yr) occurred at 1100°C. The polarization curve shows the presence of the passive area Fig. (6). The largest passive area occurred in grinding ball hardened at 900°C, at which the layers of

aluminium oxide (Al_2O_3) are the most stable. This means that the highest corrosion resistance occurred at 900°C, at which the most stable layers of aluminium oxide and the largest passive area were obtained. Besides, microstructure changes also affect the corrosion resistance of Fe-Al-Mn alloy grinding ball because the formation of the kappa phase increases its corrosion resistance.

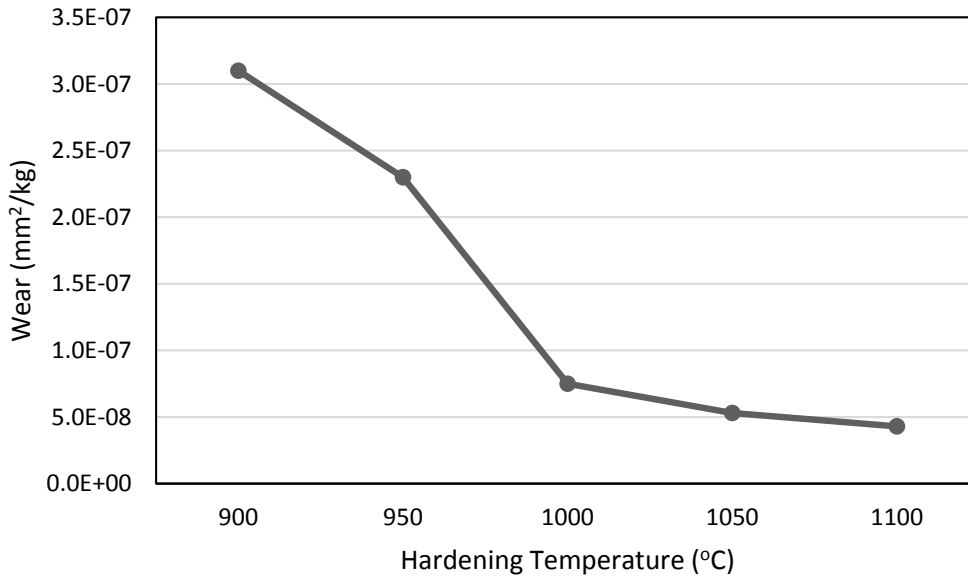


Fig. (4). Wear rate of Fe-Al-Mn grinding ball.

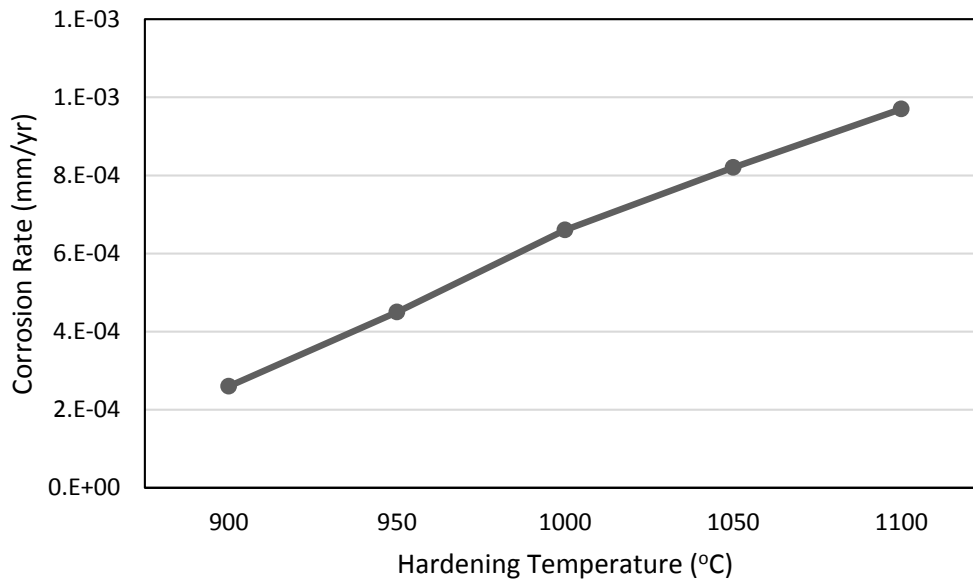


Fig. (5). The corrosion rate of Fe-Al-Mn grinding ball.

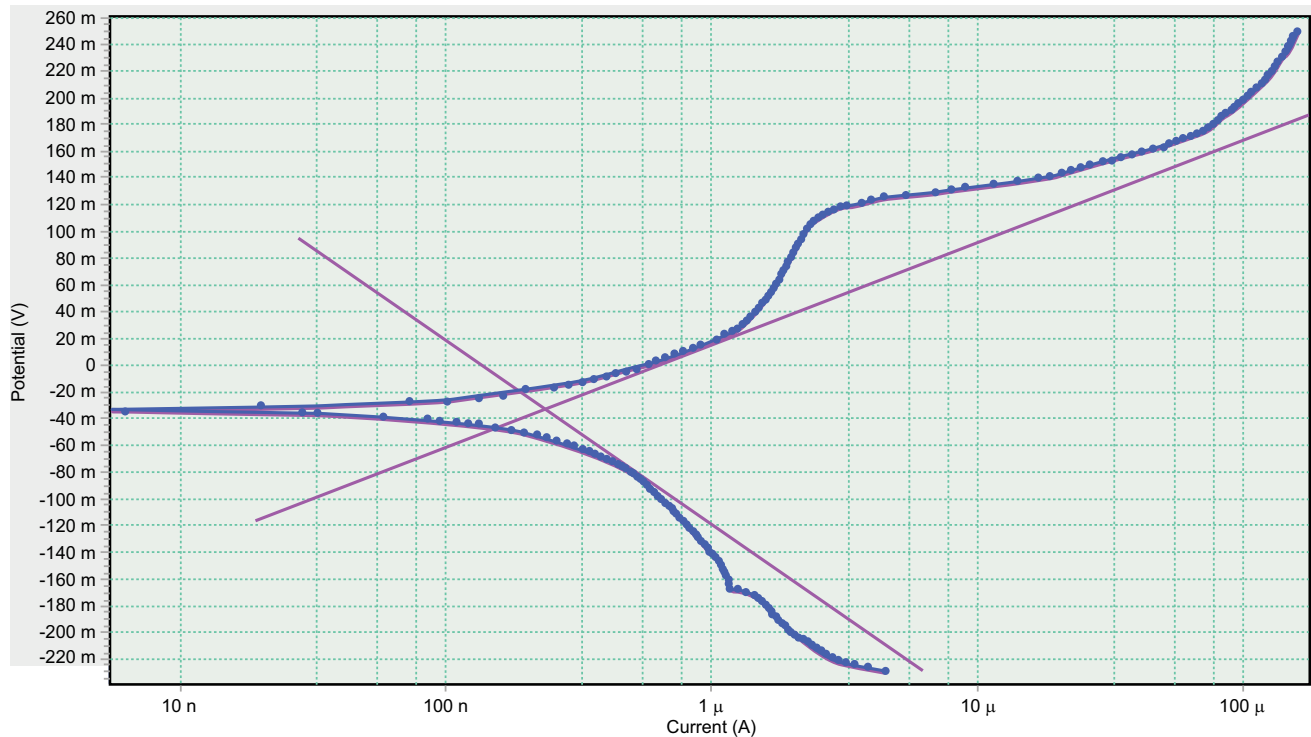


Fig. (6). Polarization curve of 950°C hardened Fe-Al-Mn grinding ball.

CONCLUSION

Microstructures of the Fe-Al-Mn alloy grinding ball after the hardening process are austenite, ferrite and kappa. The hardening process improves the wear resistance up to 4.3×10^{-7} mm³/kg and corrosion resistance in 2.5% NaCl as much as 0.00026 mm/yr at 900°C.

CONSENT FOR PUBLICATION

Not applicable.

AVAILABILITY OF DATA AND MATERIALS

Not applicable.

FUNDING

Financial support were provided by Directorate General of Research Empowerment and Development, Ministry of Research, Technology and Higher Education with “Hibah Penelitian Terapan” program (gn: 7/E/KPT/2018 and ca: 111/SP2H/LT/DRPM/2019; B/1435.24/L5/RA.00/2019).

CONFLICT OF INTEREST

The authors declare no conflict of interest, financial or otherwise.

ACKNOWLEDGEMENTS

The authors would like to thank Mechanical Engineering Department Institut Teknologi Nasional Yogyakarta.

REFERENCES

- [1] H. Mori, H. Mio, J. Kano, and F. Saito, "Ball mill simulation in wet grinding using a tumbling mill and its correlation to grinding rate", *Powder Technol.*, vol. 230, pp. 143-144, 2004. [<http://dx.doi.org/10.1016/j.powtec.2004.04.029>]
- [2] T. Ajaal, R.W. Smith, and W.T. Yen, "The Development and characterization of a ball mechanical alloying", *Can. Metall. Q.*, vol. 7, p. 41, 2002. [<http://dx.doi.org/10.1179/cm.2002.41.1.7>]
- [3] A.Y. Kuraln, and C. Ozsoy, "Identification and control of the raw material blending process in cement industry, Int", *J. Adaptive Control and Signal Process.*, vol. 18, p. 427, 2004. [<http://dx.doi.org/10.1002/acs.805>]
- [4] H. Li, W. Xu, X. Yang, and J. Wu, "Preparation of Portland cement with sugar filter as lime-based raw material", *J. Clean. Prod.*, vol. 66, p. 107, 2014. [<http://dx.doi.org/10.1016/j.jclepro.2013.11.003>]
- [5] I. Iwasaki, S.C. Riemer, J.N. Orlich, and K.A. Natarjan, "Corrosive and abrasive wear in ore grinding", *Wear*, vol. 103, p. 253, 1985. [[http://dx.doi.org/10.1016/0043-1648\(85\)90014-6](http://dx.doi.org/10.1016/0043-1648(85)90014-6)]
- [6] J.W. Jang, I. Iwasaki, and J.J. Moore, "The Effect of galvanic interaction between martensite and ferrite in grinding media wear", *Corros.*, vol. 45, p. 402, 1989. [<http://dx.doi.org/10.5006/1.3582036>]
- [7] S. Turenne, S. Lavallée, and J. Masounave, "Matrix microstructure effect on the abrasion wear resistance of high-Chromium white cast iron", *J. Mater. Sci.*, vol. 24, p. 3021, 1989. [<http://dx.doi.org/10.1007/BF02385662>]
- [8] A.S.H. Mousavi, A. Bahrami, N. Varahram, and P. Davami, "Effect of tungsten on erosion-corrosion behaviour of high chromium white cast iron", *Mater. Sci. Eng.*, vol. 623, pp. 454-455, 2007.
- [9] W.D. Bailey, and J.M. Zimmer, Patent # 4865662, Patent Genius,
- [10] G. Frommeyer, E.J. Drewes, and B. Engl, "Physical and mechanical properties of iron-aluminum-(Mn-Si) lightweight steel", *Metall. Res. Tech.*, vol. 97, p. 1245, 2000.
- [11] H. Kim, D.W. Suh, and N.J. Kim, "Fe-Al-Mn-C lightweight structural alloys: A review on the microstructures and mechanical properties", *Sci. Technol. Adv. Mater.*, vol. 14, no. 1, 2013.014205

- [http://dx.doi.org/10.1088/1468-6996/14/1/014205] [PMID: 27877553]
- [12] C.M. Liu, H.C. Cheng, C.Y. Chao, and K.L. Ou, "Phase transformation of high temperature on Fe-Al-Mn-Cr-C Alloy", *J. Alloys Compd.*, vol. 488, p. 52, 2009. [http://dx.doi.org/10.1016/j.jallcom.2009.08.072]
- [13] M. Karlík, M. Slámová, and T. Mánik, "Mánik, and Kovove, Influence of Fe and Si on the microstructure of the Al-Mn alloy with Zr addition", *Mater.*, vol. 47, p. 139, 2009.
- [14] G. Frommeyer, and Ud. Brux, "Microstructures and mechanical properties of high-strength Fe-Mn-Al-C light-weight TRIPLEX steels", *Steel Res. Int.*, vol. 77, p. 627, 2006. [http://dx.doi.org/10.1002/srin.200606440]
- [15] M.S. Chen, H.C. Cheng, C.F. Huang, C.Y. Chao, K.L. Ou, and C.H. Yu, "Microstructures and mechanical properties of high-strength Fe-Mn-Al-C light-weight TRIPLEX steels", *Mater. Charact.*, vol. 61, p. 206, 2010. [http://dx.doi.org/10.1016/j.matchar.2009.11.011]
- [16] C.M. Liu, H.C. Cheng, and K.L. Ou, "Phase transformation of high temperature on Fe-Al-Mn-Cr-C alloy", *J. Alloys Compd.*, vol. 488, p. 52, 2009. [http://dx.doi.org/10.1016/j.jallcom.2009.08.072]
- [17] C.Y. Chao, and C.H. Liu, "Effects of Mn Contents on the microstructure and mechanical properties of the Fe-10Al-xMn-1.0C alloy", *Mater. Trans.*, vol. 43, p. 2365, 2002. [http://dx.doi.org/10.2320/matertrans.43.2635]
- [18] R. Kartikasari, "Effect of mangan content on mechanical properties and corrosion behavior of as cast Fe-7.5Al-0.6C alloy", *Int J of Apl Eng Res.*, vol. 10, p. 32884, 2015.
- [19] J.E. Jin, and Y.K. Lee, "Effects of Al on Microstructure and tensile properties of C-bearing high Mn TWIP steel", *Acta Mater.*, vol. 60, p. 1680, 2012. [http://dx.doi.org/10.1016/j.actamat.2011.12.004]
- [20] K.T. Park, K.G. Jin, S.H. Han, S.W. Hwang, K. Choi, and C.S. Lee, "Stacking fault energy and plastic deformation of fully austenitic high manganese steels: Effect of Al addition", *Mater. Sci. Eng. A*, vol. 527, p. 3651, 2010. [http://dx.doi.org/10.1016/j.msea.2010.02.058]
- [21] J.S. Jeong, W. Woo, K.H. Oh, S.K. Kwon, and Y.M. Koo, "In situ neutron diffraction study of the microstructure and tensile deformation behavior in Al-added high manganese austenitic steels", *Acta Mater.*, vol. 60, p. 2290, 2012. [http://dx.doi.org/10.1016/j.actamat.2011.12.043]
- [22] K. Choi, C.H. Seo, H. Lee, S.H. Kim, J.H. Kwak, K.G. Chin, K.T. Park, and N.J. Kim, "Effect of aging on the microstructure and deformation behavior of austenite base lightweight Fe-28Mn-9Al-0.8C steel", *Scr. Mater.*, vol. 63, p. 1028, 2010. [http://dx.doi.org/10.1016/j.scriptamat.2010.07.036]
- [23] V. Rigaud, D. Daloz, J. Drillet, A. Perlade, P. Maugis, and G. Lesoult, "Phase equilibrium study in quaternary iron-rich Fe-Al-Mn-C alloys", *ISIJ Int.*, vol. 47, p. 898, 2007. [http://dx.doi.org/10.2355/isijinternational.47.898]
- [24] U.R. Kattner, and B.P. Burton, *Phase Diagrams of Binary Iron Alloys*, 2nd ed ASM International: Ohio, 1993.
- [25] M. Palm, "Concepts derived from phase diagram studies for the strengthening of Fe-Al based alloys", [http://dx.doi.org/10.1016/j.intermet.2004.10.015]
- [26] S.L. Chan, Y.L. Young, and K. Lee, "Schaeffler diagram for high Mn steels", *J. Alloys Compd.*, vol. 628, p. 46, 2015. [http://dx.doi.org/10.1016/j.jallcom.2014.12.134]
- [27] X.P. Chen, Y.P. Xu, W.J. Lee, W.Q. Chao, and Q. Liu, "Aging hardening response and β -Mn transformation behavior of high carbon high manganese austenitic low-density Fe-30Mn-10Al-2C steel", *Mater. Sci. Eng.*, vol. 703, p. 167, 2017. [http://dx.doi.org/10.1016/j.msea.2017.07.055]
- [28] D.A. Jones, *Principles and Prevention of Corrosion*, 2nd ed Prentice-Hall International: London, 1996.
- [29] G.M. Fontana, *Corrosion Engineering*, 3rd ed McGraw Hill: Singapore, 1988.